Research article

Guoce Yang, Yijie Niu, Hong Wei, Benfeng Bai* and Hong-Bo Sun

Greatly amplified spontaneous emission of colloidal quantum dots mediated by a dielectric-plasmonic hybrid nanoantenna

https://doi.org/10.1515/nanoph-2019-0332
Received August 28, 2019; revised October 19, 2019; accepted October 22, 2019

Abstract: Optical nanoantennas can efficiently harvest electromagnetic energy from nanoscale space and boost the local radiation to the far field. The dielectric-metal nanogap is a novel design that can help to overcome the core issue of optical loss in all-metal nanostructures while enabling photon density of states larger than that in all-dielectric counterparts. This article reports that a crystalline spherical silicon nanoparticle on metal film (SiNPoM) nanoantenna can largely enhance the spontaneous emission intensity of quantum dots by an area-normalized factor of 69 and the decay rate by 42-fold compared with quantum dots on glass. A high total quantum efficiency of over 80%, including ~20% for far-field radiation and ~60% for surface plasmon polaritons, is obtained in simulation. Thanks to not only the low optical loss in dielectric nanoparticles but also the appropriate gap thickness which weakens the non-radiative decay due to the quenching from metal. Mie resonant modes additionally provide the flexible control of far-field emission patterns. Such a simple optical nanoantenna can be combined with various nanoscale optical emitters and easily extended to form large area metasurfaces functioning as active regions in light-emitting devices in applications such as advanced display, wireless optical communication, and quantum technology.

Keywords: silicon nanoparticle; plasmonics; spontaneous emission; Purcell effect; nanoantenna.

1 Introduction

Spontaneous emission as a fundamental optical process has recently attracted great interest due to its potential application in various fields such as optical interconnection [1], optical wireless communication [2, 3], and quantum technology [4]. The related study is also beneficial to understand other optical emission processes such as the stimulated emission [5–7] and the two-photon emission [8, 9]. However, low brightness and slow emission rate have been bottlenecks to hinder such devices moving into practical realm. An optical antenna provides a promising solution to amplify and enhance the spontaneous emission by increasing the local density of states (LDOS) of photons in the proximity of antennas [10, 11], namely the Purcell effect [12, 13]. Besides, nanogaps in optical antennas can also create "hot spots" with large electric field enhancement to largely increase the excitation rate of emitters located in nanogaps [14, 15]. In the past years, optical antennas with nanogaps can be mainly classified into two categories; all-metal plasmonic antennas [16–22] and all-dielectric antennas [23, 24]. The formers, such as plasmonic nano-dimers [16], bowtie structures [17], nanopatch antennas [18] and nanogaps created by gold nanorods on metal film [22], have the ability to realize an extremely small mode volume via the nanogap and thus enhance the spontaneous emission rate. However, gold, as one of the commonly used plasmonic materials, introduces inevitable optical loss that strongly increases the non-radiative decay rate and thus limits the total quantum efficiency (QE) [21]. Silver nanoparticles have much lower

***Corresponding author: Benfeng Bai,** State Key Laboratory of Precision Measurement Technology and Instruments, Department of Precision Instrument, Tsinghua University, Beijing 100084, China, e-mail: baibenfeng@tsinghua.edu.cn
Guoce Yang and Hong-Bo Sun: State Key Laboratory of Precision Measurement Technology and Instruments, Department of Precision Instrument, Tsinghua University, Beijing 100084, China. https://orcid.org/0000-0002-6566-7776 (G. Yang)
Yijie Niu: Beijing National Laboratory for Condensed Matter Physics, Institute of Physics, Chinese Academy of Sciences, Beijing 100190, China; and School of Physics and Technology, Wuhan University, Wuhan 430072, China
Hong Wei: Beijing National Laboratory for Condensed Matter Physics, Institute of Physics, Chinese Academy of Sciences, Beijing 100190, China; and Songshan Lake Materials Laboratory, Dongguan, Guangdong 523808, China

intrinsic loss enabling higher QE [4, 19, 20] but still suffers from the oxidization and the quality and shape control in nano-fabrication. In contrast, all-dielectric structures have the advantage of small optical loss, but achieve only modest LDOS enhancement and cannot forbid the leakage of emitted photons into the dielectric substrate. A hybrid structure consisting of dielectric nanostructures on a metal film with a nanogap between them can reduce the dissipative loss while maintaining relatively high LDOS enhancement [25]. This dielectric-plasmonic configuration has been used for nanolaser and amplifier [5–7, 26–30]. Recently, there was a successful demonstration that the photoluminescence intensity could be amplified in a platform consisting of chemically synthesized silicon nanoparticles on metal film (SiNPoM) with quantum dots in the gap [31]. However, the very small gap results in strong quenching process due to the short distance between the quantum dots and the gold film, which limits the QE. In addition, the influence of the generated surface plasmon polaritons (SPPs) on the metal film on the QE was not explored, which might further reduce the photon radiation efficiency. Both the value and the composition of the QE are critical for the design of optoelectronic and quantum devices.

In this work, we propose an effective solution to address the above two key concerns with a SiNPoM antenna consisting of a crystalline spherical silicon nanoparticle (SiNP) situated on a gold film covered successively by a thin Al_2O_3 separation layer and a self-assembled CdSe/ZnS quantum dot monolayer (~10 nm thickness), as shown in Figure 1A. Several key figures of merit defining the emission properties are studied, including the decay rate, the QE, the far-field radiation pattern, and the emission intensity. The appropriate gap thickness between the SiNP and the metal film is critical to obtain enhanced emission decay rate and intensity, and lift the QE.

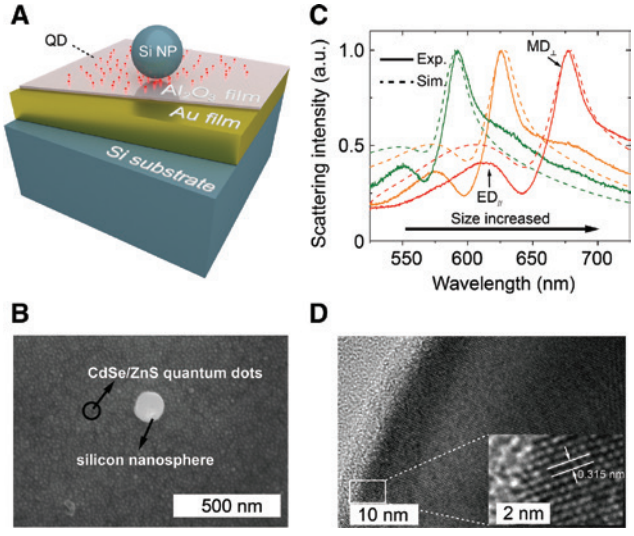

Figure 1: Silicon nanosphere on metal film nanoantenna. (A) Schematic of the SiNPoM antenna. (B) SEM image of a SiNPoM antenna with the quantum dots monolayer in the gap. (C) Measured (solid) and simulated (dashed) dark-field scattering spectra of SiNPoM antennas (with 5 nm Al_2O_3 layer) with different diameters of 162 nm (green), 174 nm (yellow) and 190 nm (red), where the resonances are red-shifted with the increase of the SiNP size. (D) High-resolution TEM image of a SiNP, reflecting the crystallinity.

2 Results and discussions

In the SiNPoM system, the sizes of CdSe/ZnS quantum dots are ~10 nm and the crystalline SiNPs are prepared by femtosecond laser ablation in liquid and the diameters are from 80 to 200 nm [32]. To prepare the sample, a 100 nm thick Au film with a 5 nm thick Cr adhesion layer was first evaporated on a silicon substrate by electron beam evaporation (0.1 nm/s for Au and 0.05 nm/s for Cr). Then a thin layer of Al_2O_3 (1–20 nm) was deposited on the top of the gold film by atomic layer deposition (ALD) with an average deposition rate of 1 nm/17 min. Afterwards, 20 µl colloidal quantum dot water solution (1×10^{-4} nmol/L) was drop on the Al_2O_3 surface and dried at room temperature. The sample was then rinsed by deionized (DI) water and dried by N_2 gas. The diluted SiNP solution was dropped on the quantum dot monolayer and rinsed by DI water after 30 min for completing adhesive assembly. Finally, after drying by N_2 gas again, a sample with sparse SiNPs situated on the quantum dot monolayer was well prepared. The gap thickness is the sum of thicknesses of the Al_2O_3 layer and the quantum dots monolayer. Figure 1B shows the scanning electron microscope (SEM) image of a single SiNPoM antenna with the quantum dots on the substrate. In the experiment, each SiNPoM antenna was characterized by dark-field scattering microscopy. The measured scattering spectra, as seen in Figure 1C, clearly show the Mie resonance features of the antennas with different sizes. In each spectrum curve, the dominant resonant peak represents the vertical (normal to the ground plane) magnetic dipole resonance $MD_\perp$ of the SiNP induced by the oblique p-polarized incident light, while the secondary peak at the shorter wavelength corresponds to the parallel electric dipole counterpart $ED_\parallel$ induced by the s-polarized light, agreeing with previous studies [33, 34]. Both resonances have red shift with the increase of SiNP size. Full-wave simulations based on the finite element method (COMSOL Multiphsyics) were conducted to get the scattering spectra (see Supplementary Material), where the refractive index of SiNP was taken from that of crystalline silicon [35] and

has a very small imaginary part. The refractive index of the gold film is modeled from Johnson and Christy's data [36]. The agreement of $MD_{\perp}$ bandwidths between the measured and the simulated spectra indicates the SiNP has low optical loss like crystalline silicon. Besides, the high-resolution transmission electron microscope (TEM) image of a SiNP shown in Figure 1D also gives the evidence of the crystallinity.

The photoluminescence (PL) intensity enhancement factor (EF) is determined by the excitation rate that can be enhanced by the local electric field at the excitation wavelength, the QE, and the collection efficiency related to the far-field emission pattern,

$$\mathrm{EF}(\mathbf{r}) = \frac{\gamma_{\mathrm{exc}}(\mathbf{r})}{\gamma^{0}_{\mathrm{exc}}} \cdot \frac{\mathrm{QE}_{\mathrm{photon}}(\mathbf{r})}{\mathrm{QE}^{0}_{\mathrm{photon}}} \cdot \frac{\eta(\mathbf{r})}{\eta^{0}} \tag{1}$$

where γ_{exc} is the excitation rate at the excitation wavelength, $\mathrm{QE}_{\mathrm{photon}}$ is the photon QE defined by $\mathrm{QE}_{\mathrm{photon}} = \gamma_{\mathrm{photon}} / (\gamma_{\mathrm{photon}} + \gamma_{\mathrm{spp}} + \gamma_{\mathrm{nr}})$, where γ_{photon} is the photon decay rate, γ_{spp} is the SPPs decay rate, γ_{nr} is the non-radiative decay rate induced by absorption of materials, η is the collection efficiency dependent on the numerical aperture (NA) of the first lens, and the superscript "0" indicates the quantities from the reference sample such as quantum dots on glass substrate. The excitation rate enhancement $\gamma_{\mathrm{exc}}/\gamma^{0}_{\mathrm{exc}}$ equals to $|\mathbf{E}_{\mathrm{exc}}|^2/|\mathbf{E}^{0}_{\mathrm{exc}}|^2$, where $\mathbf{E}_{\mathrm{exc}}$ is the electric field at the excitation wavelength. The EF is position dependent due to the inhomogeneous environment created by the antenna geometry. The measured total EF should be the average value <EF> over the excitation spot area. First, the quantum dot emitters in the nanogap underneath the SiNP get the largest excitation rate enhancement, where the maximum value can reach over 30 (Figure 2A). Besides, the presence of the SiNP results in the significantly increased LDOS and thus leads to large decay rate enhancement in the whole projection area under the SiNP despite the non-uniformity of the LDOS spatial distribution in the nanogap. The largest LDOS enhancement (>120×) occurs at the center beneath the SiNP, mainly due to the sphere-plane configuration (Figure 2B). However, the fastest decay rate does not always indicate the highest photon QE due to the absorption (non-radiative) decay and the SPPs decay channels [37]. Simulations show a photon QE of above 20% (Figure 2C). Taking the SPPs mode as a form of in-plane radiation into account, the total QE is defined as $\mathrm{QE}_{\mathrm{total}} = (\gamma_{\mathrm{photon}} + \gamma_{\mathrm{spp}}) / (\gamma_{\mathrm{photon}} + \gamma_{\mathrm{spp}} + \gamma_{\mathrm{nr}})$. Figure 2D shows the high total QE, and the pattern of the QE in the gap has a good spatial overlapping with the LDOS, so that the emitters at the center of the gap have not only the largest decay rate enhancement but also the highest QE (>80%).

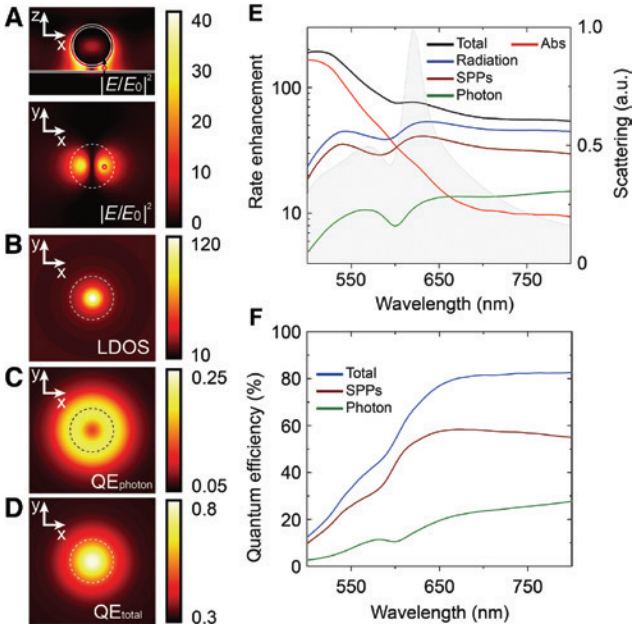

Figure 2: Electric field enhancement, LDOS enhancement, and QE in the nanogap underneath the SiNP.
(A) Simulated electric field enhancement distributions in the cross-sectional plane (upper panel) and the quantum dot monolayer plane (lower panel) of the SiNPoM at the excitation wavelength of 532 nm where the dashed line represents the projection area of the SiNP with the diameter of 174 nm and the Al_2O_3 layer is 5 nm thick. (B–D) Simulated maps of the LDOS enhancement relative to a dipole in a vacuum space (B), the photon QE (C) and the total QE (D) as a function of dipole position under the SiNP at the emission wavelength of 640 nm. (E) Simulated decay rate enhancement from various decay channels by fixing the dipole at the position of maximum excitation electric field enhancement. (F) Simulated emission wavelength dependent total QE, the SPPs QE and the photon QE.

It is obvious that emitters at the position of maximum excitation electric field will get the largest excitation rate enhancement. With the emitter fixed at this location and the emission wavelength varied, the decay rate enhancement spectra also show resonances corresponding to the Mie scattering of the antenna (Figure 2E). Absorption decays mainly happen at shorter wavelength due to the inter-band transition loss in the gold film. The metal loss monotonically and sharply decreases with the increase of emission wavelength out of the inter-band transition range, so that the total QE increases to a very high level and is no longer strongly limited by the intrinsic ohmic loss in the metal film (Figure 2F). Though the energy of SPPs dominates the aforementioned total QE, some out-coupling nanostructures, such as gratings, can help to decouple the SPPs and further lift the photon QE. Besides, the direct on-chip integration to plasmonic circuits will also benefit from such a large SPPs QE.

The far-field emission pattern of emitters coupled to an optical antenna is also important for practical applications. For example, the omnidirectional emission is useful in free-space wireless optical communications (Li-Fi), while unidirectional emission is versatile in on-chip optical interconnections. Fundamentally, the far-field emission pattern is mainly determined by the induced effective electric dipole or magnetic dipole modes. A recently developed multipole decomposition approach [38] gives a deep insight into the mechanism. There are some previous works [33, 39] investigating the scattering features of SiNPoM antennas excited by far-field illumination, showing that the induced effective dipole modes strongly depends on the polarization and incident angle of the excitation field. Hence, it is necessary to study the near-field excitation case because it is a completely different scenario. Here, the dipole emitter is placed at the position of maximum excitation field and has a vertical dipole orientation in simulation. With such an orientation, the dipole emission can be more strongly boosted through the Purcell effect compared with that in horizontal orientation. The decomposed effective electric dipole $\mathbf{p}_{\text{eff}}$ and the magnetic dipole $\mathbf{m}_{\text{eff}}$ are calculated as follows:

$$\mathbf{p}_{\text{eff}} = \int \mathbf{P}(\mathbf{r}) \mathrm{d}\mathbf{r}^3 \tag{2}$$

$$\mathbf{m}_{\text{eff}} = -\frac{\mathrm{i}\omega}{2} \int \mathbf{r} \times \mathbf{P}(\mathbf{r}) \mathrm{d}\mathbf{r}^3 \tag{3}$$

where $\mathbf{P}(\mathbf{r})$ is the polarization of antenna induced by external electromagnetic field (here is the point electric dipole source) and ω is the emission frequency. The volume integration domain encloses the entire SiNP and the gold film. The multipole decomposition results (see Figure 3) show a significant resonant phenomenon occurring in each effective dipole intensity spectrum. The effective electric dipole $\mathbf{p}_{\text{eff}}$ and the magnetic dipole $\mathbf{m}_{\text{eff}}$ have different units and their values cannot be compared directly. Considering the fact that the power ratio of an electric dipole and a magnetic dipole with the same frequency equals to $|\mathbf{p}_{\text{eff}}|^2 \cdot c^2 / |\mathbf{m}_{\text{eff}}|2$, we normalized $\mathbf{m}_{\text{eff}}$ to $\mathbf{m}_{\text{eff}}/c$ in order to make it comparable with $\mathbf{p}_{\text{eff}}$, where c is the light speed. Overall, the full spectrum can be decomposed into three regions: (i) the horizontal effective dipoles dominant resonant region (at the wavelength of around 560 nm in Figure 3A), (ii) the complex resonant region including both horizontal and vertical dipole modes (at around 620 nm in Figure 3A), and (iii) the vertical dipole dominant resonant region (at around 750 nm in Figure 3A). Quite different from the far-field excitation case, the vertical electric dipole source in the nanogap cannot induce the vertical magnetic dipole mode $\mathbf{m}_z$ any longer. A rigorous near-field to far-field transformation method [40] was used to calculate the far-field emission patterns at these three different regions (Figure 3B–D). There are good agreements between the three emission patterns and the effective dipole modes excited in the antenna. Apparently, the horizontal effective dipoles $\mathbf{p}_x$ and $\mathbf{m}_y$ generate the directional emission normal to the ground x–y plane (Figure 3B), while the vertical effective dipole $\mathbf{p}_z$ creates a butterfly-like sideward emission pattern (Figure 3D). Such a feature in the SiNPoM antenna gives a possibility to control the far-field emission pattern with more degrees of freedom in the same architecture.

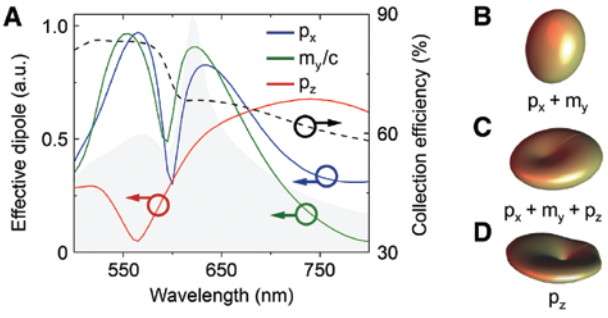

Figure 3: Multipole analysis and the far-field feature of a SiNPoM antenna.
(A) Emission wavelength dependent multipole decomposition of the emission field induced by a vertical electric dipole located at the position of maximum excitation field. (B–D) Far-field emission pattern at three typical Mie resonance wavelengths of 560 nm (B), 620 nm (C) and 750 nm (D).

In order to experimentally probe the PL intensity and the decay rate enhancement, a 532 nm continuous wave laser beam and a picosecond pulse laser beam were coupled into a microscope objective (100×) with a NA of 0.9 and focused on the antenna. The emitted light was collected by the same objective and directed into the spectrometer and the single photon avalanche detector with 550 nm long-pass filters. As shown in Figure 4, the PL spectrum exhibits dramatic amplifications: about 17-fold enhancement compared to that from quantum dots on glass, about 37-fold enhancement compared to that from quantum dots on a gold film with 5 nm Al_2O_3 spacing layer, and about 188-fold enhancement compared to that from quantum dots on a bare gold film. A figure of merit of the enhancement factor is usually normalized to the excitation spot area and the projection area of a single antenna according to

$$\mathrm{EF} = \frac{(I - I_{\text{out}})/A_{\text{antenna}}}{I_{\text{ref}}/A_{\text{spot}}} \tag{4}$$

where I is the PL counts from the SiNPoM antenna acquired by the spectrometer, I_{out} is the PL counts from

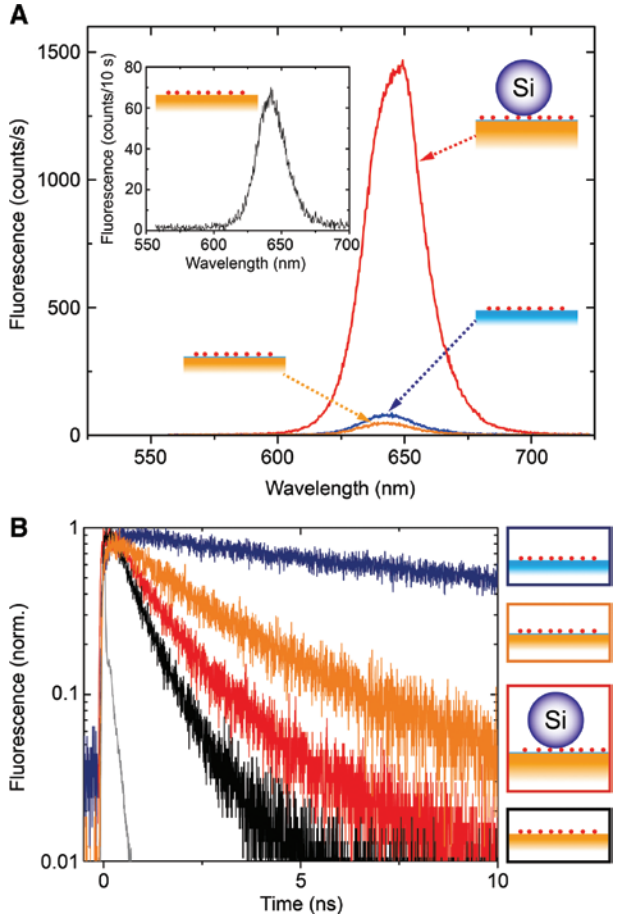

Figure 4: Enhancements of spontaneous emission intensity and decay rate.
Photoluminescence enhancement (A) and emission decay (B) from a SiNPoM antenna compared with samples as control references. Red: quantum dots coupled to a SiNPoM antenna; Blue: quantum dots on glass; Yellow: quantum dots on a gold film with 5 nm Al_2O_3 spacing layer; Black: quantum dots on a bare gold film; Grey in (B): Instrument response function.

the area within the laser spot but outside the SiNP projection area, I_{ref} is the counterpart from the reference sample, $A_{antenna}$ is the projection area of the SiNP, and A_{spot} is the excitation laser spot size (here the spot diameter is around 360 nm). Here, I_{out} is defined by $I_{out} = I_{bg} \cdot (A_{spot} - A_{antenna})/A_{spot}$, where I_{bg} is the PL counts measured from the area without the SiNP. The enhancement factor defined by Eq. (4) removes the influence of quantum dots in the laser spot but not underneath the SiNP. Using Eq. (4), we can obtain the enhancement factors as 69, 115, and 826 compared to the above three different aforementioned references. It is worth noting that the normalized enhancement factor of 826 is comparable to and even larger than the previously reported value [31] even if a much thicker gap (15 nm) in our sample is used. The measured decay curves in Figure 4B show that the emission from quantum dots coupled to a SiNPoM antenna are significantly boosted compared with the quantum dots on glass, indicating a decay rate enhancement factor of 13. The total decay rate with the presence of the nanogap is also accelerated, compared with quantum dots on a gold film with 5 nm Al_2O_3 spacing layer. Although the decay rate of quantum dots on a bare gold film is even faster, the emission intensity is quite low mainly owing to the dominant non-radiative decay.

The gap thickness plays an important role in all-metal plasmonic structures. But how it influences the emission from the SiNPoM antenna is still not clear. We first investigated the gap thickness dependence of the excitation rate and the QE in theory. In simulations the intrinsic QE of 30% of quantum dot colloids used in experiments was taken into account. As seen in Figure 5, simulations show that the average excitation rate monotonically decreases with the increase in the gap thickness due to the weakened excitation field (Figure 5A), while the average total QE has the most opposite trend and remains over 70% for the gap thickness larger than 20 nm. On the other hand, the photon QE reaches the maximum when the gap thickness approaches 20 nm (Figure 5B). The collection efficiency into a NA of 0.9 is above 75%, much larger than 17% from a glass sample, and does not have a significant change for different gap thickness (Figure 5C). Hence, the total PL intensity enhancement curve does not vary much for gap thickness less than 15 nm but drops much for thickness larger than 20 nm combining all above influences. The experimentally measured PL intensity enhancement for samples with different gap thicknesses shows good agreements with the simulation results as shown in Figure 5D. To further demonstrate the ability of the SiNPoM antenna to control and boost the decay rate, time-resolved emission measurements were proceeded with samples with different gap thicknesses. As shown in Figure 5E and F, apparently, the decay rates in all samples are enhanced and increase with the decrease of gap thickness, which coincides with the theoretical predictions. The measured largest decay rate enhancement of 42-fold corresponding to the fitted lifetime of 330 ps occurs on the sample with a 10 nm gap and meanwhile the PL intensity is also enhanced by a factor about 10 relative to the glass sample. Even faster decay can be achieved using thinner gap and the PL enhancement is maintained. Such a good feature makes it possible to be applied in fast modulation with optical pump. On the other hand, without considering the excitation rate enhancement by optical pump, both the total QE and the photon QE reach almost the maxima at the gap thickness of 20 nm with the decay rate enhanced by about 10-fold, which could be applied towards brighter

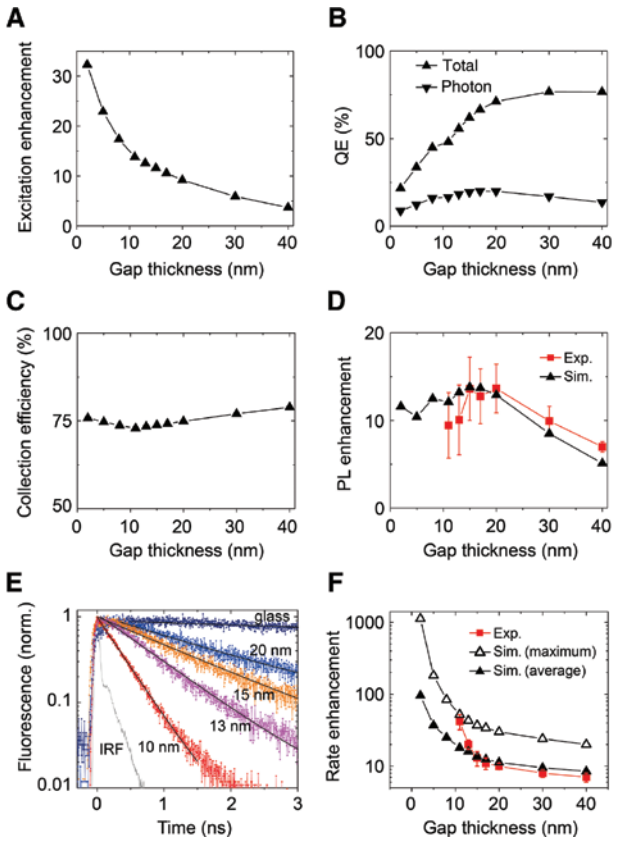

Figure 5: Gap thickness dependence of PL intensity and decay rate enhancement.
(A) Simulated average excitation rate enhancement for emitters in the gap compared to those on glass as a control. (B) Simulated average total QE and photon QE. (C) Simulated average collection efficiency into the NA of 0.9. (D) Measured and simulated total PL enhancement relative to quantum dots on glass as a function of the gap thickness (measured as the PL peak intensity ratio without area normalization). The simulated enhancement for each gap thickness is obtained by averaging over the excitation laser spot with the diameter of 360 nm. The excitation power density is 20 W/cm^2 in all measurements. (E) Measured time-resolved emission decay curves for varied gap thicknesses, where the measured curves (in different colors) are fitted by a single-exponential function and represented by black lines. (F) Measured and simulated decay rate enhancement as a function of the gap thickness, where the simulated results include the maximum rate enhancement and the average counterpart over the excitation spot area.

and faster electrical pump light-emitted devices, and efficient single photon sources with high radiative rate.

3 Conclusions

In summary, the investigated SiNPoM antenna is shown to be a powerful platform for the control of various spontaneous emission properties with the high intensity, fast decay, high QE, and desirable radiation pattern. We experimentally showed that a large decay rate enhancement with a factor of 42 corresponding to a lifetime of 330 ps is obtained from a sample with the smallest gap of 10 nm and the largest photoluminescence (PL) amplification factor of 17 is obtained from a sample with a 15 nm gap, both of which are compared with quantum dots spread on a glass substrate as reference. A high QE over 80% is obtained in simulations, including a photon QE of 20% and a SPPs QE of 60%. Smaller gap size leads to sharply increased decay rate but the gap thickness less than 15 nm will significantly increase the quenching effect and thus reduce the QE contributed to the fluorescence intensity. Such a simple structure can be readily scaled to a large area forming novel light-emitting metasurfaces, which can be used in advanced optoelectronic devices and efficient quantum sources operating at any interested wavelength as long as appropriate size of the SiNP is designed. Furthermore, such a hybrid integration between low-loss dielectric nanoparticles and various plasmonic films could be extended to boost emission processes in a broader spectral region such as epsilon-near-zero materials in the infrared region and graphene monolayer in the terahertz region.

Acknowledgments: Authors Guoce Yang and Benfeng Bai would like to acknowledge the support provided by the National Natural Science Foundation of China (Grant No. 61775113, Funder Id: http://dx.doi.org/10.13039/501100001809). Yijie Niu and Hong Wei. acknowledge for the support by the Ministry of Science and Technology of China (Grant No. 2015CB932400) and the National Natural Science Foundation of China (Grant No. 11774413, Funder Id: http://dx.doi.org/10.13039/501100001809). All authors thank Prof. Guowei Yang at School of Materials Science and Engineering, Sun Yat-sen University, Guangzhou, China, for providing the colloidal silicon nanospheres prepared by femtosecond laser ablation in liquid.

References

[1] Tsakmakidis KL, Boyd RW, Yablonovitch E, Zhang X. Large spontaneous-emission enhancements in metallic nanostructures: towards LEDs faster than lasers [invited]. Opt Express 2016;24:17916–27.
[2] Islim MS, Ferreira RX, He X, et al. Towards 10 Gb/s orthogonal frequency division multiplexing-based visible light communication using a GaN violet micro-LED. Photon Res 2017;5:A35–43.

[3] Dregely D, Lindfors K, Lippitz M, Engheta N, Totzeck M, Giessen H. Imaging and steering an optical wireless nanoantenna link. Nat Commun 2014;5:4354.
[4] Hoang TB, Akselrod GM, Mikkelsen MH. Ultrafast room-temperature single photon emission from quantum dots coupled to plasmonic nanocavities. Nano Lett 2016;16:270–5.
[5] Ma RM, Oulton RF. Applications of nanolasers. Nat Nanotechnol 2019;14:12–22.
[6] Wang S, Wang XY, Li B, et al. Unusual scaling laws for plasmonic nanolasers beyond the diffraction limit. Nat Commun 2017;8:1889.
[7] Oulton RF, Sorger VJ, Zentgraf T, et al. Plasmon lasers at deep subwavelength scale. Nature 2009;461:629–32.
[8] Rivera N, Kaminer I, Zhen B, Joannopoulos JD, Soljacic M. Shrinking light to allow forbidden transitions on the atomic scale. Science 2016;353:263–9.
[9] Rivera N, Rosolen G, Joannopoulos JD, Kaminer I, Soljacic M. Making two-photon processes dominate one-photon processes using mid-IR phonon polaritons. Proc Natl Acad Sci 2017;114:13607–12.
[10] Novotny L, Van Hulst N. Antennas for light. Nat Photonics 2011;5:83–90.
[11] Muhlschlegel P, Eisler HJ, Martin OJF, Hecht B, Pohl DW. Resonant optical antennas. Science 2005;308:1607–9.
[12] Purcell EM. Spontaneous emission probabilities at radio frequencies. Phys Rev 1946;69:681.
[13] Yablonovitch E. Inhibited spontaneous emission in solid-state physics and electronics. Phys Rev Lett 1987;58:2059–62.
[14] Xu H, Bjerneld EJ, Kall M, Borjesson L. Spectroscopy of single hemoglobin molecules by surface enhanced raman scattering. Phys Rev Lett 1999;83:4357–60.
[15] Xu H, Aizpurua J, Kall M, Apell P. Electromagnetic contributions to single-molecule sensitivity in surface-enhanced raman scattering. Phys Rev E 2000;62:4318–24.
[16] Andersen SKH, Kumar S, Bozhevolnyi SI. Ultrabright linearly polarized photon generation from a nitrogen vacancy center in a nanocube dimer antenna. Nano Lett 2017;17:3889–95.
[17] Kinkhabwala A, Yu Z, Fan S, Avlasevich Y, Mullen K, Moerner WE. Large single-molecule fluorescence enhancements produced by a bowtie nanoantenna. Nat Photonics 2009;3:654–7.
[18] Ciraci C, Rose A, Argyropoulos C, Smith DR. Numerical studies of the modification of photodynamic processes by film-coupled plasmonic nanoparticles. J Opt Soc Am B 2014;31:2601–7.
[19] Akselrod GM, Argyropoulos C, Hoang TB, et al. Probing the mechanisms of large Purcell enhancement in plasmonic nanoantennas. Nat Photonics 2014;8:835–40.
[20] Hoang TB, Akselrod GM, Argyropoulos C, Huang J, Smith DR, Mikkelsen MH. Ultrafast spontaneous emission source using plasmonic nanoantennas. Nat Commun 2015;6:7788.
[21] Shen Q, Boyce AM, Yang G, Mikkelsen MH. Polarization-controlled nanogap cavity with dual-band and spatially overlapped resonances. ACS Photonics 2019;6:1916–21.
[22] Sugimoto H, Yashima S, Fujii M. Hybridized plasmonic gap mode of gold nanorod on mirror nanoantenna for spectrally tailored fluorescence enhancement. ACS Photonics 2018;5:3421–7.
[23] Regmi R, Berthelot J, Winkler PM, et al. All-dielectric silicon nanogap antennas to enhance the fluorescence of single molecules. Nano Lett 2016;16:5143–51.
[24] Cihan AF, Curto AG, Raza S, Kik PG, Brongersma ML. Silicon mie resonators for highly directional light emission from monolayer MoS2. Nat Photonics 2018;12:284.
[25] Yang Y, Miller OD, Christensen T, Joannopoulos JD, Soljacic M. Low-loss plasmonic dielectric nanoresonators. Nano Lett 2017;17:3238–45.
[26] Ma RM, Oulton RF, Sorger VJ, Bartal G, Zhang X. Room-temperature sub-diffraction-limited plasmon laser by total internal reflection. Nat Mater 2011;10:110–3.
[27] Lu YJ, Kim J, Chen HY, et al. Plasmonic nanolaser using epitaxially grown silver film. Science 2012;337:450–3.
[28] Zhang Q, Li G, Liu X, et al. A room temperature low-threshold ultraviolet plasmonic nanolaser. Nat Commun 2014;5:4953.
[29] Liu N, Gocalinska A, Justice J, et al. Lithographically defined, room temperature low threshold subwavelength red-emitting hybrid plasmonic lasers. Nano Lett 2016;16:7822–8.
[30] Liu N, Wei H, Li J, et al. Plasmonic amplification with ultra-high optical gain at room temperature. Sci Rep 2013;3:1967.
[31] Sugimoto H, Fujii M. Broadband dielectric-metal hybrid nanoantenna: Silicon nanoparticle on a mirror. ACS Photonics 2018;5:1986–93.
[32] Yan J, Liu P, Lin Z, et al. Directional fano resonance in a silicon nanosphere dimer. ACS Nano 2015;9:2968–80.
[33] Kuo YL, Chuang SY, Chen SY, Chen KP. Enhancing the interaction between high-refractive index nanoparticles and gold film substrates based on oblique incidence excitation. ACS Omega 20161:613–9.
[34] Miroshnichenko AE, Evlyukhin AB, Kivshar YS, Chichkov BN. Substrate-induced resonant magnetoelectric effects for dielectric nanoparticles. ACS Photonics 2015;2:1423–8.
[35] Palik ED. Handbook of optical constants of solids. San Diego, CA, USA: Academic Press, 1998.
[36] Johnson PB Christy RW. Optical constants of the noble metals. Phys Rev B 1972;6:4370.
[37] Li Q, Wei H, Xu H. Quantum yield of single surface plasmons generated by a quantum dot coupled with a silver nanowire. Nano Lett 2015;150:8181–7.
[38] Evlyukhin AB, Reinhardt C, Evlyukhin E, Chichkov BN. Multipole analysis of light scattering by arbitrary-shaped nanoparticles on a plane surface. J Opt Soc Am B 2013;30:2589–98.
[39] Sinev I, Iorsh I, Bogdanov A, et al. Polarization control over electric and magnetic dipole resonances of dielectric nanoparticles on metallic films. Laser Photonics Rev 2016;10:799–806.
[40] Yang J, Hugonin JP, Lalanne P. Near-to-far field transformations for radiative and guided waves. ACS Photonics 2016;3:395–402.

Supplementary Material: The online version of this article offers supplementary material (https://doi.org/10.1515/nanoph-2019-0332).